J. Quant. Spectrosc. Radiat. Transfer Vol. 32, No. 4, pp. 325–333, 1984
Printed in Great Britain

0022-4073/84 $3.00 + .00

PREDICTION AND ASSIGNMENT OF THE FIR SPECTRUM OF HYDROGEN PEROXIDE†

PAUL HELMINGER
Department of Physics, University of South Alabama, Mobile, AL 38866, U.S.A.

and

J. K. MESSER, WAYNE C. BOWMAN‡ and FRANK C. DE LUCIA
Department of Physics, Duke University, Durham, NC 27706, U.S.A.

(*Received* 28 *December* 1983)

Abstract—Millimeter and submillimeter microwave studies are used to predict and assign the FIR rotational–torsional spectrum of hydrogen peroxide. Special attention is given to the strong Q-branch features that have recently been used by Traub and Chance to place an upper limit on the atmospheric abundance of hydrogen peroxide. In addition, 67 new transitions are reported in the 400–1000 GHz region.

1. INTRODUCTION

Hydrogen peroxide occurs commonly in a variety of important physical and chemical systems including those associated with upper atmospheric and combustion processes. Waters *et al.*[1] have reported a tentative observation of HOOH in the stratosphere by means of a balloon-borne millimeter wave emission experiment. More recently, Chance and Traub,[2] using FIR techniques, report an upper limit on the stratospheric content of this species. These measurements are especially important because HOOH plays an important role in stratospheric HO_x chemistry.[3]

The geometrical simplicity of hydrogen peroxide belies its spectroscopic complexity. HOOH is a light asymmetric rotor with substantial centrifugal distortion and internal rotation effects. This spectroscopic richness has provided the basis for a large number of infrared studies.[4–9] A number of years ago, Massey *et al.*[10,11] observed two microwave lines of HOOH and Oelfke and Gordy[12] measured 50 millimeter-wave transitions.

More recently, we measured more than 200 new lines, mostly in the submillimeter wave region.[13,14] All 283 lines of the high resolution microwave, millimeter wave, and submillimeter wave data set were then analyzed. One of the most important results of our work was the demonstration of a technique that made possible the analysis of this very large data set to microwave accuracy $\sim 0.000003\ cm^{-1}$. This technique has now been used to analyze modern high resolution infrared spectra, which also requires that proper treatment be given to asymmetric rotor centrifugal distortion theory as well as to the effects of internal rotation.[9] Hillman has also used this approach in a reanalysis of our data that simultaneously varies ground and excited torsional state constants.[15]

For a model to be of maximum usefulness for the interpretation of remote sensing data, it must not only account for observed laboratory data, but it must also accurately predict the spectrum of the species over a wide spectral range. The rotational–torsional spectrum of HOOH extends to much higher frequency than the experimental range of our earlier experimental studies. It provides a rich FIR spectrum with a number of strong features that are due to a near degeneracy in certain Q-branch frequencies. These are the features used by Chance and Traub[2] in their balloon borne experiment. These authors have also pointed out that similar features exist in HOCl and HO_2[15] and other slightly asymmetric rotors.

In this paper, we report the results of calculations based upon our model and our earlier microwave measurements. We compare these calculations with a laboratory FIR spectrum of Chance and Traub, with special emphasis on the unresolved structure of the strong

†Work Supported by NASA Grant NSG-7540.
‡Present address: Bell Laboratories, Room 6E111A, Whippany, NJ 07981, U.S.A.

Q-branch features. This is important for the establishment of a quantitative relation between the observed FIR feature and the atmospheric concentration of HOOH. In addition, we report the measurement of 67 new HOOH transitions in the 400–1000 GHz region and compare them with the results of our calculations.

2. THEORETICAL CONSIDERATIONS AND OVERVIEW

We have previously discussed our spectroscopic analysis technique for the rotation–torsional spectrum of HOOH.[13] Briefly, HOOH is a light, nearly prolate asymmetric rotor with internal rotation. We have extensively discussed the application of Watson's[17] reduced centrifugal distortion theory to molecules without internal motions.[18–20] The internal rotation of HOOH splits its ground vibrational state into 4 torsional states, of which the $\tau = 1, 2$ and $\tau = 3, 4$ are effectively degenerate pair wise. The splitting between these pairs is $\sim 11\ \text{cm}^{-1}$. The selection rules are such that each allowed transition requires both a torsional transition between $\tau = 1$ and 3 or $\tau = 2$ and 4 and a rotational transition that obeys c-type selection rules. In addition, symmetry considerations restrict the rotational states that exist in each torsional state. Figure 1 shows in the form of a FORTRAT diagram the rotational–torsional spectrum of HOOH in the microwave region.

Although we label all of our transitions according to standard asymmetric rotor notation, we have also grouped the transitions into branches, retaining the earlier branch designations, which are used in Fig. 1. The transitions are divided into three principal branches, according to the change in J, each denoted by P ($\Delta J = -1$), Q ($\Delta J = 0$), or R ($\Delta J = +1$). The principal P, Q, and R branches are further divided as follows: a subscript denotes the initial value of K, a superscript denotes the change in K by a P ($\Delta K = -1$) or R ($K = +1$), a U (upper) or L (lower) denotes the asymmetry splitting, and the 1←3 or 4←2 notation denotes the change in torsional state.

Theoretical consideration would lead to the expectation that cross terms in the Hamiltonian between rotation and torsion would require a complex and difficult analysis. To the contrary, our earlier work has shown that the effects of this interaction are either negligible or very strongly correlated with terms in the asymmetric rotor Hamiltonian. Thus, it was shown that it is possible to fit a large and statistically significant data set to microwave accuracy by simply allowing the upper ($\tau = 3, 4$) and lower ($\tau = 1, 2$) torsional levels to each have their own set of effective rotational constants. The effects of internal rotation are

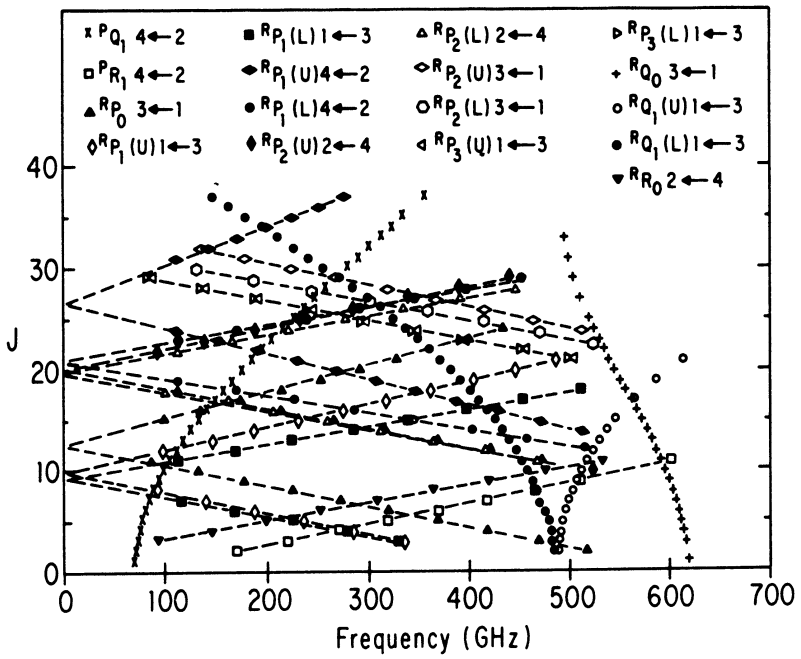

Fig. 1. FORTRAT diagram of hydrogen peroxide.

accounted for by assigning a single splitting energy to the difference between the pairs of torsional states.

This result has been confirmed and extended by Hillman[15] in a reanalysis of our microwave data, and by Hillman *et al.*[9] and Olson and Hunt[20] in analyses of i.r. spectra.

3. SPECTRAL OVERVIEW

Although an analysis of HOOH to microwave accuracy requires careful attention to the details discussed above, a useful, semi-quantitative picture of the observed FIR spectrum can be obtained from simple theory. For the higher values of K that occur in the FIR, the asymmetry splitting is not usually resolved and the molecule approximates a symmetric top. In this aproximation, the rotational energy is given by

$$E_r = \tfrac{1}{2}(B + C)J(J + 1) + [A - \tfrac{1}{2}(B + C)]K^2, \tag{1}$$

and, for Q-branches ($\Delta J = 0$), the frequencies are

$$\nu_Q = [A - \tfrac{1}{2}(B + C)](K_f^2 - K_i^2) \approx 9.209\,(K_f^2 - K_i^2)\,\mathrm{cm}^{-1}. \tag{2}$$

The torsional splitting (11.437 cm^{-1}) is then either added or subtracted. Since this expression is not a function of J, in this approximation all of the different J transitions are degenerate. In practice, this is a good approximation as can be seen by comparing the predictions of this expression with the observed FIR spectra.[2,7] For $\Delta J = \pm 1$ (P and R branches) this J degeneracy is lifted and $\pm(B + C)(J + 1)$ added to the frequency expression. In the FIR spectrum, these lines are much weaker because they are well resolved and the J-degeneracy associated with the Q-branch does not exist. Thus, for each value of K (except 0) there are 12 branches that arise from: (1) the K degeneracy that leads to the asymmetry splitting, (2) the torsional splitting, and (3) the P, Q, and R branches. Thus, ${}^RQ_5(U)4\leftarrow 2$ designates the upper asymmetry component of a branch for which $\Delta J = 0$, the initial value of K is 5, the final value of K is 6, and which starts in one of the lower ($\tau = 2$) torsional levels and ends in one of the upper ($\tau = 4$) torsional levels. Because K is large, the asymmetry splitting is essentially zero and the upper and lower components of ${}^RQ_5 4\rightarrow 2$ are degenerate.

It is useful to make a semi-quantitative comparison between the form of the spectrum predicted by this approximate theory and the experimental results of Hunt *et al.*[7] and Chance and Traub.[2] At the resolution of Hunt *et al.* ($\sim 0.3\,\mathrm{cm}^{-1}$), the most prominent features are the Q-branches which result from the contributions of many unresolved lines. As shown above, these occur in pairs split by twice the torsional energy. Figure 2 shows

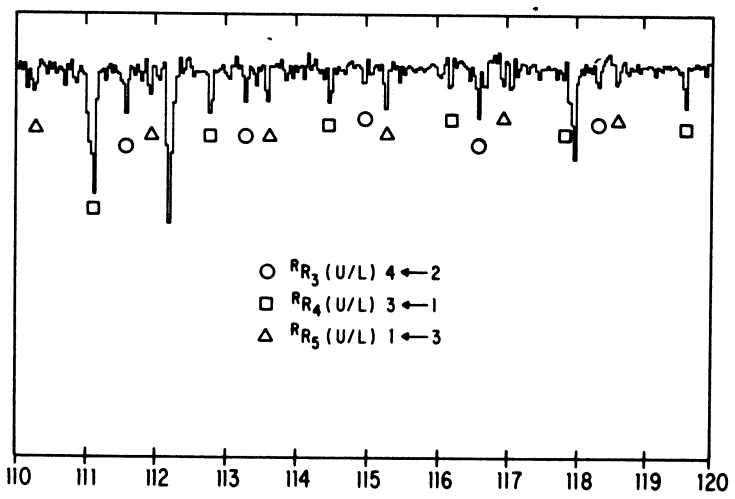

Fig. 2. The FIR spectrum between 110 cm^{-1} and 120 cm^{-1}.

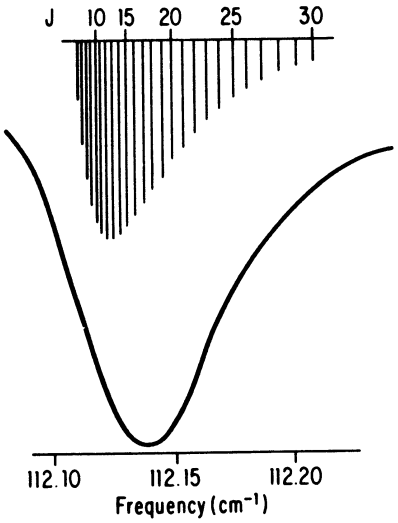

Fig. 3. Structure of the Q-Branch near 112 cm^{-1}.

the 110 cm^{-1} to 120 cm^{-1} region of the spectrum of Chance and Traub at a resolution of $\sim$0.03 cm^{-1}. Inspection of this spectrum shows a strong Q-branch feature ($^RQ_5(U/L)4\leftarrow2$) near 112 cm^{-1}. The simple theory predicts, and the data of Hunt *et al.* show, its companion ($^RQ_5(U/L)1\leftarrow3$) lower in frequency by twice the torsional splitting

Table 1. Prediction of $^RR_4(U/L)$ branch from submillimeter analysis (cm^{-1}).

Transition $\tau = 3$ — $\tau = 1$	Predicted	O. - P.
5(5, 1) - 4(4, 1)	102.517	0.001
6(5, 2) - 5(4, 2)	104.228	-0.002
7(5, 3) - 6(4, 3)	105.939	0.004
8(5, 4) - 7(4, 4)	107.650	0.007
9(5, 5) - 8(4, 5)	109.361	-0.003
10(5, 6) - 9(4, 6)	111.071	H_2O[a]
11(5, 7) - 10(4, 7)	112.780	0.002
12(5, 8) - 11(4, 8)	114.489	-0.000
13(5, 9) - 12(4, 9)	116.198	-0.001
14(5,10) - 13(4,10)	117.905	0.002
15(5,11) - 14(4,11)	119.612	0.002
16(5,12) - 15(4,12)	121.318	H_2O[a]
17(5,13) - 16(4,13)	123.023	0.003
18(5,14) - 17(4,14)	124.727	-0.003
19(5,15) - 18(4,15)	126.429	-0.005
20(5,16) - 19(4,16)	128.131	-0.002
21(5,17) - 20(4,17)	129.831	0.002
22(5,18) - 21(4,18)	131.529	0.004
23(5,19) - 22(4,19)	133.226	-0.001
24(5,20) - 23(4,20)	134.921	0.008
25(5,21) - 24(4,21)	136.615	-0.004

[a] A strong H_2O impurity line obscures the HOOH line.

($\sim 23\,cm^{-1}$), near $89\,cm^{-1}$. This feature is not present in the spectrum of Chance and Traub. The explanation of this requires the more detailed analysis presented in the next section.

Also shown in Fig. 2 are numerous small features. These, and other similar features (~ 1000) in the rest of the spectrum, we will later demonstrate to be assignable individual P or R branch transitions.

4. RESULTS

It was our original intention to include the FIR data in our fit in order to improve the quality of the analysis and to eliminate the extrapolation problems. However, because we could find no systematic deviations between our calculated spectrum and the observed FIR spectrum and because these deviations were typically of the order of the expected experimental uncertainty ($\sim 0.003\,cm^{-1}$), this was not done. Thus, we simply assign the FIR spectrum between $40\,cm^{-1}$ and $220\,cm^{-1}$ on the basis of our submillimeter ($<25\,cm^{-1}$) analysis. This process also eliminates the need to make difficult decisions about blended lines, etc.

The Q-branch near $112\,cm^{-1}$ has recently been used to place an upper limit on stratospheric HOOH in a balloon borne experiment of Chance and Traub. Figure 3 shows this feature in the laboratory spectrum on an expanded scale along with the prediction of our analysis for $T = 300$ K. The curve comes directly from their computer output which shows the details of the lineshape at 10 times the resolution of Fig. 2. It can be seen that the agreement is very good. It should be noted that because the components of the feature extend over about a resolution element of the instrument, that the peak of the theoretical

Table 2. Prediction of ${}^{R}R_5(U/L)$ branch from submillimeter analysis (cm^{-1}).

Transition τ = 1 — τ = 3	Predicted	O. - P.
6(6, 1) - 5(5, 1)	100.118	-0.001
7(6, 2) - 6(5, 2)	101.814	-0.002
8(6, 3) - 7(5, 3)	103.507	0.002
9(6, 4) - 8(5, 4)	105.197	0.009
10(6, 5) - 9(5, 5)	106.885	-0.000
11(6, 6) - 10(5, 6)	108.570	-0.006
12(6, 7) - 11(5, 7)	110.251	0.000
13(6, 8) - 12(5, 8)	111.930	-0.006
14(6, 9) - 13(5, 9)	113.605	-0.006
15(6,10) - 14(5,10)	115.276	-0.002
16(6,11) - 15(5,11)	116.944	-0.004
17(6,12) - 16(5,12)	118.607	-0.006
18(6,13) - 17(5,13)	120.267	-0.003
19(6,14) - 18(5,14)	121.922	H_2O[a]
20(6,15) - 19(5,15)	123.573	-0.019
21(6,16) - 20(5,16)	125.219	0.006
22(6,17) - 21(5,17)	126.860	-0.024
23(6,18) - 22(5,18)	128.495	-0.016
24(6,19) - 23(5,19)	130.126	-0.016
25(6,20) - 24(5,20)	131.750	H_2O[a]

[a] A strong H_2O impurity line obscures the HOOH line.

Table 3. Newly observed submillimeter transitions of HOOH(MHz).

$^{R}R_0$ Branch

Transition	Frequency		
τ = 3 τ = 1	Observed	Predicted	O. - P.
1(1, 0) - 0(0, 0)	670595.82	670595.83	-0.01
2(1, 1) - 1(0, 1)	722904.94	722905.00	-0.06
3(1, 2) - 2(0, 2)	775711.43	775711.68	-0.25
4(1, 3) - 3(0, 3)	829018.01	829018.17	-0.16
5(1, 4) - 4(0, 4)	882829.27	882829.27	0.00
6(1, 5) - 5(0, 5)	937152.57	937152.45	0.12

$^{R}R_0$ Branch

Transition	Frequency		
τ = 2 τ = 4	Observed	Predicted	O. - P.
13(1,12) - 12(0,12)	647108.62	647108.35	0.27
14(1,13) - 13(0,13)	705794.26	705794.07	0.19
15(1,14) - 14(0,14)	765078.56	765078.42	0.14
16(1,15) - 15(0,15)	824977.94	824977.85	0.09

$^{R}Q_0$ Branch

Transition	Frequency		
τ = 3 τ = 1	Observed	Predicted	O. - P.
2(1, 2) - 2(0, 2)	617459.18	617459.11	0.07
26(1,26) - 26(0,26)	514903.72	514903.84	-0.12
28(1,28) - 28(0,28)	507068.19	507068.29	-0.10
30(1,30) - 30(0,30)	500752.69	500752.86	-0.17
32(1,32) - 32(0,32)	496179.73	496179.97	-0.24
33(1,33) - 33(0,33)	494603.00	494603.36	-0.36
34(1,34) - 34(0,34)	493523.48	493524.11	-0.63
35(1,35) - 35(0,35)	492955.53	492956.54	-1.01
36(1,36) - 36(0,36)	492910.73	492912.35	-1.62
37(1,37) - 37(0,37)	493398.19	493400.72	-2.53

$^{R}P_0$ Branch

Transition	Frequency		
τ = 3 τ = 1	Observed	Predicted	O. - P.
24(1,23) - 25(0,25)	463402.63	463402.82	-0.19
25(1,24) - 26(0,26)	494509.65	494509.92	-0.27
26(1,25) - 27(0,27)	524351.52	524351.95	-0.43
27(1,26) - 28(0,28)	552900.67	552901.28	-0.61
28(1,27) - 29(0,29)	580133.20	580133.95	-0.75
29(1,28) - 30(0,30)	606028.96	606029.85	-0.89
30(1,29) - 31(0,31)	630571.92	630572.99	-1.07

(*Contd.*)

Table 3. (*Contd.*)

$^{P}R_{1}$ Branch

Transition		Frequency		
τ = 2	τ = 4	Observed	Predicted	O. - P.
9(1, 8) -	10(0,10)	556103.13	556103.07	0.06
11(1,10) -	12(0,12)	647026.29	647026.20	0.09
12(1,11) -	13(0,13)	691505.59	691505.46	0.13
13(1,12) -	14(0,14)	735300.93	735300.79	0.14
14(1,13) -	15(0,15)	778389.41	778389.13	0.28

$^{R}R_{1}$ Lower Branch

Transition		Frequency		
τ = 1	τ = 3	Observed	Predicted	O. - P.
2(2, 0) -	1(1, 0)	587991.70	587991.66	0.04
3(2, 1) -	2(1, 1)	638278.48	638278.47	0.01
4(2, 2) -	3(1, 2)	688065.63	688065.60	0.03
5(2, 3) -	4(1, 3)	737362.55	737362.49	0.06
6(2, 4) -	5(1, 4)	786181.78	786181.51	0.27

$^{R}R_{1}$ Upper Branch

Transition		Frequency		
τ = 1	τ = 3	Observed	Predicted	O. - P.
2(2, 1) -	1(1, 1)	588932.17	588932.14	0.03
3(2, 2) -	2(1, 2)	641094.12	641094.00	0.12
4(2, 3) -	3(1, 3)	693682.09	693681.98	0.11
5(2, 4) -	4(1, 4)	746693.64	746693.71	-0.07
6(2, 5) -	5(1, 5)	800126.81	800126.84	-0.03

(*Contd. on next page*)

stick spectrum should not coincide exactly with the peak of the unresolved line. The details of this unresolved structure are important for the interpretation of field data because the relative strengths of the components vary greatly with temperature. Our calculations show that while the individual linestrengths of the components of the companion Q-branch near 89 cm^{-1} are about the same as those in the 112 cm^{-1} component, that they are spread over a much wider spectral region. Specifically, a typical spacing in the 89 cm^{-1} feature is about 0.03 cm^{-1} and in the 112 cm^{-1} feature only about 0.003 cm^{-1}. This result, which is due to the small differences between the upper ($\tau = 3, 4$) state and lower ($\tau = 1, 2$) state spectral constants, causes the feature near 89 cm^{-1} to effectively disappear at the higher resolution of the Chance and Traub instrument. This situation exists for all of the Q-branch pairs, so that only the upper member of the pair produces a strong feature at the higher resolution of Chance and Traub.

Also shown in Fig. 2 are the identifications of the portions of the ${}^{R}R_{3}(U/L)4\leftarrow2$, ${}^{R}R_{4}(U/L)3\leftarrow1$, and ${}^{R}R_{5}(U/L)1\leftarrow3$ branches that fall in the region. Each of the observed lines is in fact an unresolved asymmetry split K-doublet. Since each of these pairs contains both a statistical weight 1 and statistical weight 3 line, the intensity alteration that would be expected for molecules of this symmetry is not observed. To give an idea of the quality both of the predictions and experimental data, Tables 1 and 2 show numerical comparisons for the ${}^{R}R_{4}(U/L)3\leftarrow1$ and ${}^{R}R_{5}(U/L)1\leftarrow3$ branches. These comparisons are based upon spec-

Table 3. (*Contd.*)

$^{R}P_{1}$ Lower Branch

Transition		Frequency		
τ = 4	τ = 2	Observed	Predicted	O. - P.
6(2, 4) -	7(1, 6)	796809.81	796809.43	0.38
7(2, 5) -	8(1, 7)	741612.59	741612.27	0.32
8(2, 6) -	9(1, 8)	686004.75	686004.60	0.15
9(2, 7) -	10(1, 9)	630012.22	630011.87	0.35
10(2, 8) -	11(1,10)	573662.97	573662.45	0.52

$^{R}P_{1}$ Upper Branch

Transition		Frequency		
τ = 4	τ = 2	Observed	Predicted	O. - P.
6(2, 5) -	7(1, 7)	826748.38	826747.82	0.56
7(2, 6) -	8(1, 8)	780023.08	780022.55	0.53
8(2, 7) -	9(1, 9)	733897.97	733897.68	0.29
9(2, 8) -	10(1,10)	688380.55	688380.24	0.31
10(2, 9) -	11(1,11)	643477.80	643477.62	0.18
11(2,10) -	12(1,12)	599198.02	599197.70	0.32

$^{R}P_{2}$ Lower Branch

Transition		Frequency		
τ = 2	τ = 4	Observed	Predicted	O. - P.
6(3, 3) -	7(2, 5)	678322.05	678322.27	-0.22
7(3, 4) -	8(2, 6)	626609.05	626608.92	0.13
8(3, 5) -	9(2, 7)	574810.12	574810.24	-0.12
9(3, 6) -	10(2, 8)	522913.61	522913.70	-0.09
28(3,25) -	29(2,27)	505188.39	505188.59	-0.20

$^{R}P_{2}$ Upper Branch

Transition		Frequency		
τ = 2	τ = 4	Observed	Predicted	O. - P.
4(3, 2) -	5(2, 4)	781614.83	781614.56	0.27
5(3, 3) -	6(2, 5)	730120.50	730120.64	-0.14
6(3, 4) -	7(2, 6)	678609.32	678609.31	0.01
7(3, 5) -	8(2, 7)	627086.84	627087.00	-0.16
8(3, 6) -	9(2, 8)	575560.67	575560.71	-0.04
30(3,28) -	31(2,30)	538510.07	538510.29	-0.22
31(3,29) -	32(2,31)	587129.94	587130.39	-0.45
32(3,30) -	33(2,32)	635467.82	635468.03	-0.21
33(3,31) -	34(2,33)	683509.73	683510.05	-0.32

trometer output which shows the experimental spectrum with a plotting density 10 times higher than that shown in Fig. 2. Inspection of these Tables shows that the agreement is ordinarily much better than 0.01 cm^{-1}. In many of the poorer cases, we have predicted nearly degenerate overlaps from other lines. Presumably, most of the remaining larger deviations are due to overlaps from unassigned lines in excited torsional states. The agreements shown here are typical for the stronger R- and P-branches that are expected to have minimal problems associated with blended lines. This general level of agreement exists throughout the entire spectral region and extends to levels of about $K = 7$. Above this, the assignments become less certain, largely because the density of lines of that intensity approaches unity.

In addition, we have measured 67 new microwave transitions in the frequency region between 400 and 1000 GHz. These transitions are in the most favorable region for microwave based measurements of the atmosphere and are shown in Table 3. Also shown in this Table are the frequencies calculated from our earlier analysis. Inspection shows that many of them are predicted to about experimental uncertainty, but that some of them show measurable deviations from our predictions.

5. CONCLUSIONS

In this paper, we have shown that the analysis technique that we have developed for the rotational–torsional spectrum of hydrogen peroxide is capable of excellent predictions of the FIR spectrum. This is especially remarkable because hydrogen peroxide is a light asymmetric rotor with internal rotation and because the range of extrapolation from the input microwave data set to the predicted FIR spectrum is almost an entire order of magnitude. From the point of view of atmospheric science, the most important result of these calculations is that they provide the detailed structure of the strong Q-branch features. This information is necessary for the interpretation of intensities, especially in situations where the temperatures may vary. Finally, we report 67 new submillimeter transitions, bringing to a total of 350 the number of microwave lines that have now been observed and assigned.

REFERENCES

1. J. W. Waters, J. C. Hardy, R. F. Jarnot, and H. M. Pickett, *Science* **214**, 61 (1981).
2. K. V. Chance and W. A. Traub, to be published.
3. J. G. Anderson, *Causes and Effects of Stratospheric Ozone Reduction: An Update*. National Academy Press, Washington (1982).
4. O. Bain and P. A. Giguere, *Can. J. Chem.* **33**, 527 (1955).
5. D. Chin and P. A. Giguere, *J. Chem. Phys.* **34**, 690 (1961).
6. R. L. Redington, W. B. Olson, and P. C. Cross, *J. Chem. Phys.* **36**, 1311 (1962).
7. R. H. Hunt, R. A. Leacock, C. W. Peters, and K. T. Hecht, *J. Chem. Phys.* **42**, 1931 (1965).
8. D. Goorvitch, F. P. J. Valero, F. S. Bonomo, and P. M. Sivaggio, *JQSRT* **27**, 575 (1982).
9. J. J. Hillman, D. E. Jennings, W. B. Olson, and A. Goldman, *37th Symp. Molecular Spectroscopy, RE*12, Columbus, Ohio (1982).
10. J. T. Massey and D. R. Bianco, *J. Chem. Phys.* **22**, 442 (1954).
11. J. T. Massey and R. W. Hart, *J. Chem. Phys.* **23**, 942 (1955).
12. W. C. Oelfke and W. Gordy, *J. Chem. Phys.* **51**, 5336 (1965).
13. P. Helminger, W. C. Bowman, and F. C. De Lucia, *J. Molec. Spectrosc.* **85**, 120 (1981).
14. W. C. Bowman, F. C. De Lucia, and P. Helminger, *J. Molec. Spectrosc.* **87**, 571 (1981).
15. J. J. Hillman, *J. Molec. Spectrosc.* **95**, 236 (1982).
16. K. V. Chance and W. A. Traub, *JQSRT* **29**, 81 (1983).
17. J. K. G. Watson, *J. Chem. Phys.* **45**, 1360 (1966).
18. P. Helminger, R. L. Cook, and F. C. De Lucia, *J. Molec. Spectrosc.* **40**, 125 (1971).
19. F. C. De Lucia, R. L. Cook, P. Helminger, and W. Gordy, *J. Chem. Phys.* **55**, 5334 (1971).
20. R. L. Cook, F. C. De Lucia, and P. Helminger, *J. Molec. Spectrosc.* **41**, 123 (1972).
21. W. B. Olson and R. Hunt, *38th Symp. Molecular Spectroscopy, WE*13, Columbus, Ohio (1983).